CONF-860605--28

A COMPOSITE MODEL OF MICROSTRUCTURAL EVOLUTION IN AUSTENITIC STAINLESS STEEL UNDER FAST NEUTRON IRRADIATION*

R. E. Stoller
Metals and Ceramics Division
Oak Ridge National Laboratory
Oak Ridge, TN 37831

and

G. R. Odette
University of California
Santa Barbara, CA

MASTER

CONF-860605--28

DE87 000018

ABSTRACT

A rate-theory-based model has been developed which includes the simultaneous evolution of the dislocation and cavity components of the microstructure of irradiated austenitic stainless steels. Previous work has generally focused on developing models for void swelling while neglecting the time dependence of the dislocation structure. These models have broadened our understanding of the physical processes that give rise to swelling, e.g., the role of helium and void formation from critically-sized bubbles. That work has also demonstrated some predictive capability by successful calibration to fit the results of fast reactor swelling data. However, considerable uncertainty about the values of key parameters in these models limits their usefulness as predictive tools. Hence the use of such models to extrapolate fission reactor swelling data to fusion reactor conditions is compromised.

The present work represents an effort to remove some of these uncertainties by self-consistently generating the time dependence of the dislo-

*Research sponsored by the Division of Materials Sciences, U.S. Department of Energy, under contract DE-AC05-84OR21400 with Martin Marietta Energy Systems, Inc. and the Office of Fusion Energy, U.S. Department of Energy, under contract AM03-765F00034 with the University of California at Santa Barbara. Partial support for one of the authors (Stoller) was provided by the U.S. DOE Magnetic Fusion Energy Technology Fellowship Program administered by the Oak Ridge Associated Universities.

By acceptance of this article, the publisher or recipient acknowledges the U.S. Government's right to retain a nonexclusive, royalty-free license in and to any copyright covering the article.

DISTRIBUTION OF THIS DOCUMENT IS UNLIMITED

cation structure, both faulted loops and network dislocations. The model's predictions reveal the closely coupled nature of the evolution of the various microstructural components and generally track the available fast reactor data in the temperature range of 350–700°C for doses up to 100 dpa. As the theoretical model has become more complex, parameter choices were constrained to a more limited range of values in order to obtain this agreement between theory and experiment. While the model remains approximate in many respects, it should ultimately provide a more useful tool for understanding microstructural evolution under irradiation and permit more confident predictions of void swelling in future fusion reactors.

INTRODUCTION

The task of predicting the observable effects of neutron irradiation of stainless steel is hindered by the complex interactions of numerous microscopic phenomena (1,2). A rigorous treatment requires that one consider the simultaneous evolution of the various microstructural features and microchemical effects such as solute segregation and irradiation induced phase instabilities. Parameters such as effective point defect biases are difficult to quantify precisely, yet they play a major role in determining the nucleation and growth rates of the various extended defects.

Development of theoretical models is further hindered by an incomplete data base and large heat-to-heat variations in microstructural data. Such variations may in part be related to effects such as reactor duty differences during various experiments or uncertainties in the temperature, flux, and fluence at which the experiment was conducted. However, type 316

stainless steel has also shown a significant sensitivity to subtle changes in minor alloying elements (e.g. carbon, titanium, and silicon) (3) and details of thermo-mechanical treatment. Such sensitivity increases the uncertainty in determining values for certain critical physical parameters, such as "effective" diffusion coefficients and the recombination coefficient. Further, model predictions are not unique in that various combinations of mechanisms and parameters can result in "reasonable" agreement with the data. This is particularly a problem if interpretation of limited data sets, containing intrinsic uncertainties, are interpreted in terms of single or few mechanisms. Unfortunately such interpretations are often further compromised by only qualitatively considering the underlying mechanisms and by failing to consider the statistical significance of so-called data trends. Single mechanism models can be very important in developing an understanding of individual processes; however, they can justifiably be applied in quantitative analysis only if both rigorous control over experimental variables is maintained and if it can be shown that the interaction of multiple mechanisms is not important. This is not often the case in practice. However, empirical approaches may still provide an engineering expedient for data correlation and some limited extrapolation of data.

More complex quantitative models allow for competition and interaction of mechanisms which have been identified, but they suffer from the proliferation of non-unique parameters as noted above. Hence, they are most effective as analytical tools only if the possible ranges of parameter combinations are identified and considered in any extrapolation. Two important components of any data analysis effort are the explicit recognition of

the likely non-uniqueness of any single calibration and a quantitative effort to ascertain the consequences of this in extrapolated predictions. This general problem has been discussed in some detail previously (1).

The model described below is part of an overall effort to develop a quantitative understanding of microstructural evolution in irradiated alloys. The model focuses on the coupled evolution of the major microstructural features observed in irradiated austenitic stainless steels; bubbles, voids, faulted dislocation loops and network dislocations. The effects of second phase precipitate particles are included to a limited degree. The effects of microchemical evolution, which is known to occur and is likely to be of importance, are not explicitly treated. However, the influence of microchemical evolution is approximately accounted for in the various rate theory parameters. The major approximation here is in the use of material parameters (e.g. biases and diffusivities) which are not altered to reflect either spatial or temporal fluctuations in the alloy composition.

DESCRIPTION OF THE MODEL

The model developed here is an extension of previous work which examined primarily the evolution of the cavity component of the irradiated microstructure (4–8). That work helped to establish the generally accepted sequence of events which lead to void swelling; viz., that bubbles nucleate and slowly grow by accumulating both vacancies and helium until they reach a critical size, r^*, which is determined by the vacancy supersaturation, S,

the material parameters γ, the surface energy and Ω, the atomic volume and temperature, T.

$$r^* = f(\ell n\ S)\ \frac{\gamma\Omega}{kT\ell nS} \qquad (1)$$

The function $f(\ell n\ S)$ is a non-ideal gas correction factor (8); for an ideal gas $f = 4/3$ and k is Boltzman's constant. After reaching this critical size the bubbles are converted to voids and begin to grow primarily by vacancy accumulation. Similar theoretical work by others has also confirmed this general scenario (9–11). Since references 6 and 7 describe the cavity evolution model in detail, it will not be discussed further here.

Calculation of Point Defects Concentrations

The approach used to calculate the point defect concentrations follows the familiar rate theory (7,12). The conventional rate equations which describe the vacancy and interstitial concentrations are slightly modified due to the dislocation evolution models. The following assumptions are implicit in the mathematical description:

1. The concentrations of vacancies and mono-, di-, tri-, and tetra-interstitials are calculated as if they were at steady state during a given time step.
2. Only the mono-defects are mobile. Mobility of small clusters has been shown to have no significant effect on the point defect calculations (13). A relatively high interstitial migration energy (0.85 eV) is

used. This value is consistent with recent measurements of this parameter in austenitic steels (14,15). Solute-interstitial trapping could account for this value.

3. The tetra-interstitial is the stable nucleus for Frank faulted loop growth The di- and tri-interstitials may thermally dissociate by emitting single interstitials.

4. The point defect sinks included are bubbles, voids, subgrain structure, transient vacancy clusters in the form of microvoids as a result of cascade collapse, network dislocations and Frank faulted loops. The sink strengths are calculated using a first order effective medium approach as described previously (7). The faulted loop and network dislocations preferentially absorb interstitials; all other sinks are unbiased.

The rate equations then are:

$$\frac{dC_v}{dt} = G_v - \beta_v^2 C_2 - \beta_v^3 C_3 - \beta_v^4 C_4 - \alpha C_i C_v - D_v C_v (S_v^n + S_v^\ell + S_v^c + S_v^{vcl} + S_v^g) \qquad (2)$$

$$\frac{dC_i}{dt} = \eta G_{dpa} + C_2(2E_2^i + \beta_v^2 - \beta_i^2) + C_3^d(E_3^i - \beta_i^3) - \beta_i^1 C_1 - \beta_i^4 C_4$$

$$- \alpha C_i C_v - D_i C_i (S_i^n + S_i^\ell + S_i^c + S_i^{vcl} + S_i^g) \qquad (3)$$

$$\frac{dC_2}{dt} = \beta_i^1 \frac{C_i}{2} + C_3(\beta_v^3 + E_3^i) - C_2(\beta_v^2 + \beta_i^2 + E_2^i) \qquad (4)$$

$$\frac{dC_3}{dt} = \beta_i^2 C_2 + \beta_v^4 C_4 - C_3(\beta_v^3 + \beta_i^3 + E_3^i) \tag{5}$$

$$\frac{dC_4}{dt} = \beta_i^3 C_3 - \beta_v^4 C_4 - C_4\ \tau_4^{-1} \tag{6}$$

In Eqs. (2–6) C_2, C_3, and C_4 are concentrations of di-, tri-, and tetra-interstitials, the $\beta_{i,v}^j$ and $E_{2,3}^i$ are rate constants for the impingement of point defects on interstitial clusters of size j and the thermal dissociation of di- and tri-interstitials, respectively, $S_{i,v}^{\ell}$ is the faulted loop sink strength and τ_4 will be discussed below. The other terms have their normal meaning (see Table 1).

$$\beta_{i,v}^j = \frac{z_{i,v} D_{i,v} C_{i,v}}{a_o^2} \tag{7}$$

$$E_{2,3}^i = \frac{D_i}{a_o^2} \exp\left(-\frac{E_{2,3}^b}{kT}\right) \tag{8}$$

$$S_{i,v}^{\ell} = \frac{2\pi}{\ell n(r_o/r_c)} \sum_j 2\pi r_{\ell}^j N_{\ell}^j Z_{i,v}(r_{\ell}^j) \tag{9}$$

The $Z_{i,v}^{\ell}(r_{\ell})$ are faulted loop bias factors for interstitials and vacancies and r_c and r_o are the dislocation core radius and the outer cutoff radius, respectively. The outer cutoff radius is taken as the mean dislocation spacing, $r_o = (\pi\rho_n)^{-1/2}$, and the core radius is twice the Burgers vector, $r_c = 2b_{\ell}$ (16,17). Values for the binding energy of the second and third interstitial in a cluster ($E_{2,3}^b$) and for the combinatorial numbers ($z_{i,v}^j$) in Eq. (7) are given in Table 2. The choice of these values will be discussed below.

The vacancy generation rate (G_v) is computed by summing the contributions from each sink type (S_j).

$$G_v = \eta G_{dpa}(1 - \chi) + D_v \sum S_j C_v^j \tag{10}$$

The C_v^j in Equation (10) are the vacancy concentrations in equilibrium with the appropriate sink. These have been given previously (7) with the exception of C_v^ℓ, the value for faulted loops.

$$C_v^\ell(r_\ell) = C_v^e \exp[-\frac{\Omega}{kT}(\frac{G_s b_\ell}{4\pi(1-\upsilon)r_\ell} \ell n (\frac{4r_\ell}{b_\ell}) + \frac{\gamma_{sf}}{b_\ell})] \tag{11}$$

The first term in the exponential in Eq. (11) is the elastic energy opposing loop growth due to the increasing dislocation line length while the second term is due to the stacking fault; G_s is the shear modulus (18), υ is Poisson's ratio, γ_{sf} is the stacking fault energy and b_ℓ is the magnitude of the Burgers vector ($b_\ell = a_o/\sqrt{3}$).

Faulted Loop Evolution

The present model distinguishes between the small interstitial clusters and the larger faulted loops by treating their evolution differently. The τ_4 term in Eq. (6) is the lifetime of a tetra-interstitial against growth to the size of the first faulted loop size class. If r_4 is the radius of the tetra-interstitial and r_1^ℓ is the radius of loops in the first size class,

$$\tau_4 = \int_{r_4}^{r_1^\ell} (\frac{dr_\ell}{dt})^{-1} \, dr_\ell \tag{12}$$

$$\frac{dr_\ell}{dt} = \frac{A}{b_\ell}\left[Z_i^\ell(r_\ell)D_iC_i - Z_v^\ell(r_\ell)D_v(C_v - (C_v^\ell(r_\ell))\right] \quad (13)$$

in which $A = 2\pi/\ell n(r_o/r_c)$ and C_v^ℓ is given by Equation (11).

The use of the term $C_4\tau_4^{-1}$ in Eq. (6) permits a transition between regions in which alternate descriptions of interstitial loop evolution are used. As shown in Eqs. (4–6), a discrete clustering calculation is done for sizes up to the tetra-interstitial. However, this description would necessitate integrating greater than 10^4 rate equations if it were used for loops up to the maximum size observed experimentally. The evolution of the larger loops is instead given by equations of the form

$$\frac{dN_i^\ell}{dt} = N_{i-1}^\ell\tau_i^{-1} - N_i^\ell\tau_{i+1}^{-1} \quad (14)$$

where N_i^ℓ is the number of loops in a given size class with radius r_i^ℓ and the τ_i are given by Eq. (12) with the appropriate radii used as the limits of the integration. The loop size distribution between r_4 and the maximum loop radius is divided into a histogram which preserves the essential features of the distribution. The number of size classes required can be determined numerically. Figure 1 is a plot of the loop density and loop line length at 450°C as a function of the number of size classes used. These predictions are essentially independent of the number of size classes when more than about 15 size classes are used.

It remains to be shown that Eq. (6) provides a numerically appropriate boundary condition between the two regions. This can be done by comparing the net forward current (J_+) from Eq. (6) with a more rigorous calculation based on the continuity equation. The continuity equation yields the following result:

$$\frac{\partial}{\partial t}(n(r)) = -\frac{\partial}{\partial r}(\dot{r}n(r)) \tag{15}$$

$$\approx \frac{-\dot{r}(r + \delta r)n(r + \delta r) + \dot{r}(r)n(r)}{\delta r} .$$

If $r = r_4$, $r + \delta r = r_5$, $n(r) = C_4$ and $n(r + \delta r) = C_\ell$; then Eq. (15) yields:

$$J_+ = \frac{\dot{r}(C_4)C_4}{\delta r} \tag{16}$$

$$J_+ = \frac{C_4 b_\ell}{A(r_5 - r_4)} [Z_i^\ell(r_4)D_iC_i - Z_v^\ell(r_4)D_v(C_v - C_v^\ell(r_4)] \tag{17}$$

where Eq. (13) has been substituted for $\dot{r}(C_4)$. Alternately, J_+ from Eq. (6) is given by $C_4\tau_4^{-1}$.

$$C_4\tau^{-1} = C_4 / \frac{A}{b_\ell} \int_{r_4}^{r_1^\ell} [Z_i^\ell(r_\ell)D_iC_i - Z_v^\ell(r_\ell)D_v(C_v - C_v^\ell(r_\ell))]^{-1} \, dr \tag{18}$$

$$C_4\tau_4^{-1} = \frac{C_4 b_\ell}{A} \frac{1}{(r_1^\ell - r_4)} [Z_i^\ell(r_4)D_iC_i - Z_v^\ell(r_4)D_v(C_v - C_v^\ell(r_4)] \tag{19}$$

where the integral has been approximately evaluated by the values of the integrand at the lower limit times dr. In the limit as r_1^ℓ approaches r_5 (the radius of the penta-interstitial), Eqs. (17) and (19) are equal by inspection. This equality is subject to the assumption that the integrand in Eq. (18) is only a weak function of r. This condition is met by noting that $D_vC_v^\ell(r_\ell) \sim 0$ for small loops and that in the present model the biases are not size dependent

as discussed elsewhere (19). Finally, it is worth noting that the values in Fig. 1 for 32 size classes correspond to the case where $r_1^{\ell} = r_5$.

Network Dislocation Evolution

The model for the evolution of the dislocation structure includes four components, two of which are solely due to the irradiation and two of which are thermal. The thermal components are a high temperature climb source term (Bardeen-Herring sources) and a thermal annihilation term due to stress-assisted directional diffusion of vacancies. Models of this type have been developed for the study of creep processes (20,21). Network dislocations can be recovered by climb and glide processes leading to annihilation. The present model assumes that climb is the rate controlling process. The climb velocity of an edge dislocation subject to a stress, σ, is given by Nix et. al. (22) as

$$v_{cl}^{\sigma} = \frac{2\pi}{\ell n(r_o/r_c)} \frac{\Omega}{bKT} D_v C_v^e \sigma \ . \tag{20}$$

Adopting the model of Gibbs (23), the stress is assumed to be an internal (back) stress due to a population of immobilized dislocations

$$\sigma = AGb\rho_i^{1/2} \tag{21}$$

where A is nominally 0.4 and ρ_i is the density of pinned dislocations. The average climb distance is taken as the mean dislocation spacing

$$d_{cl} = (\pi\rho_n)^{-1/2} \ . \tag{22}$$

Using Eqs. (20–22) one obtains a lifetime against annihilations due to this climb-glide process as

$$\tau_{th} = \frac{d_{cl}}{v_{cl}^{\sigma}} = \left[A' \frac{2\pi^{3/2}}{\ell n(r_o/r_c)} \frac{\Omega G D_v C_v^e}{kT} \rho_n \right]^{-1} . \qquad (23)$$

In Eq. (23) $A\rho_i^{1/2}$ has been set to $A'\rho_n^{1/2}$ and the parameter A' was used to fit thermal recovery data.

The Bardeen-Herring sources for network dislocations are similar to the Frank-Read source except that the former are climb driven while the later are glide driven (24). The source is shown schematically in Fig. 2 in which a pinned dislocation segment is bowed due to an applied stress. After climbing a sufficient distance, the source will collapse leaving a dislocation loop and the original line segment which can generate succeeding loops. For simplicity, the source may be assumed to generate $2\pi L$ of new dislocation line length after climbing a distance L. The time to generate this new line length (τ_{gen}) is defined by analogy with Eq. (23). The climb velocity is given by Eq. (20) and the generation rate is then

$$R_{th}^{\rho_n} = \frac{2\pi L}{\tau_{gen}} S_D = \frac{2\pi L v_{cl}^{\sigma}}{L} S_D \qquad (24)$$

$$R_{th}^{\rho_n} = 2\pi v_{cl}^{\sigma} S_D \qquad (25)$$

in which S_D is the source density. In cold worked materials potential sources of this type include not only the dislocation network but also the subgrain structure. The parameter S_D was also used as a fitting parameter.

The thermal dislocation source and annihilation terms were calibrated using tensile data obtained at 450°, 550°, and 650°C for AISI 316 stainless steel. This data included yield strength measurements (2% offset) for both 20% cold-worked and solution annealed material as well as 20% cold worked material aged

for 4000 hours at the test temperature (25). Assuming that the hardening increment due to network dislocations varies as $(\rho_n)^{-1/2}$ (26) and that this is the primary cause of the increased yield strength of the cold-worked material relative to the solution annealed material, the ratios shown in Table 3 are obtained from the data. The model's predictions for these same ratios are also listed and the agreement is very good. These values are also consistent with transmission electron microscope observations on the same heat of steel after thermal aging (27). These were obtained by computing the dislocation evolution with $G_{dpa} = 0$ in the model. The parameters used to obtain these results are listed below in Table 4. They are discussed further in the section on Model Predictions.

Under irradiation, the growth and unfaulting of Frank loops provides an additional source of dislocations. The model assumes that the maximum loop size is governed by the geometrical constraint that the loop unfaults upon contacting another loop or network dislocation, hence

$$r^{\ell}_{unf} = (\pi\rho_t)^{-1/2} \qquad (26)$$

where ρ_t is the total dislocation density (28). As the loops grow into this size class, they are no longer considered Frank loops and a dislocation line length $2\pi r^{\ell}_{unf} N^{\ell}_{unf}$ is added to the dislocation network. The time constant for this process is given by Eq. (12) with the appropriate limits of integration. The rate at which new dislocation line length is generated by this mechanism is:

$$R^{\rho_n}_{irr} = 2\pi r^{\ell}_{unf} N^{\ell}_{unf} \tau^{-1} \quad . \qquad (27)$$

Network dislocations can also be annihilated by bias driven climb of point defects generated by irradiation. The climb velocity for this process is

$$v_{cl}^{irr} = \frac{1}{b_d} \left[Z_i^n D_i C_i - Z_v^n D_v (C_v - C_v^n) \right] , \qquad (28)$$

where the superscript n denotes the relevant parameter for network dislocations. By reasoning similar to that which leads to Eq. (23), the dislocation lifetime for this process is

$$\tau_{irr} = \frac{(\pi \rho_n)^{1/2}}{b_d} \left[Z_i^n D_i C_i - Z_v^n D_v (C_v - C_v^n) \right] . \qquad (29)$$

The lifetimes given in Eqs. (23) and (29) are added using an electrical resistance analog to yield the total lifetime of network dislocations,

$$\tau_T = (\tau_{irr}^{-1} + \tau_{th}^{-1})^{-1} . \qquad (30)$$

This finally leads to a rate equation describing the evolution of the dislocation network as

$$\frac{d\rho_n}{dt} = 2\pi (v_{cl}^{\sigma} S_D + r_{unf}^{\ell} N_{unf}^{\ell} \tau_{unf}^{-1}) - \rho_n \tau_T^{-1} . \qquad (31)$$

MODEL PREDICTIONS AND COMPARISON WITH DATA

Parameter Choices

There are at least two general goals in developing models such as have just been described. One is to try to develop an understanding of the important physical processes that lead to microstructural evolution under irradiation and the other is to ultimately provide some predictive capability. The satisfaction

of both of these goals is frustrated by a lack of well known material parameters for austenitic stainless steel. In some cases, measurements made on pure metals can be used to provide initial estimates, but key parameters are known to be sensitive to alloy composition and perhaps impurities (12,13,29–32). Simple void swelling models have been successfully used to explain much of the available swelling data and have provided considerable insight into the mechanisms responsible for this phenomenon (4–10); however, the ability to do predictive work with these models is compromised by uncertainty about parameter values. For example, when bulk recombination is ignored and dislocations are the major point defect sink, the vacancy supersaturation takes the following simple form (5).

$$S = \frac{\eta G_{dpa}}{S_i^n D_v C_v}(Z_i^n - 1) \qquad (32)$$

Values of the cascade efficiency (η) between 0.1 and 1.0 have been used by various workers (7,10,33) and values of the interstitial/dislocation bias (Z_i^n) have varied between ~1.02 to > 1.5 (7,34,35). Depending on the values chosen for these two parameters, the computed supersaturation can vary significantly.

The parameters used to compute the results given below are listed in Tables 2 and 4. The initial choice for most of these parameters was the value used previously (7); these values generally fall within the range of what might be termed "typical" for the void swelling models which have been referred to above. A notable exception is the relatively high activation energy for

interstitial diffusion. Measurements of E_i^m in pure metals have indicated a lower value, <0.5 eV (36). Such a value has normally been used in void swelling models already discussed; however, the results obtained from these models are not sensitive to the value of E_i^m (37). The results obtained with the present model are dependent on E_i^m via its influence on the predicted faulted loop population and their subsequent effect on network dislocation density. The value of E_i^m = 0.85 given in Table 2 is in agreement with recent measurements of this parameter in austenitic steels (14,15). The fact that the model requires such a value is encouraging. As the model became more complex, through the introduction of additional physical mechanisms, more parameters were introduced. However, the model also became somewhat "stiffer" with respect to arbitrary parameter choices. The example, reference to Eq. 32 indicates that relative changes in Z_i^n and n can be used to offset one another in a simple model. This is no longer the case in the present model since the various sinks have different dependencies on these parameters. The cavity and dislocation evolution are not independent but are coupled in a complex way via their mutual effect on the point defect concentrations.

There are several parameters used in the present work which have not been included previously. These include the thermal dislocation evolution parameters in Equations 20–25 and the parameters used in the rate equations for interstitial clusters, Equations (2–6, 9–11). The choice of the values for interstitial clustering parameters was guided by the results of more detailed nucleation calculations (13,38,39). The model's predictions are not too sensitive to the values of the combinatorial numbers while the di- and tri-interstitial binding

energies affect primarily the temperature dependence of the faulted loop density. The predicted dislocation density is sensitive to the thermal dislocation evolution parameters (Table 2) only for temperatures above about 550°C when faulted loops cease to contribute significantly to the dislocation network. To a first approximation, the source density, S_D, should be about equal to L^{-3} where L is the mean spacing of dislocation pinning points. If other dislocations provide the primary pinning sites, then L should be roughly proportional to $\rho_n^{-1/2}$. In this case, the maximum and minimum values of S_D given in Table 4 would correspond to pinned dislocation densities of 1.6×10^{14} and 7.4×10^{12} m^{-2}.

Model Predictions

The results given here were obtained using the parameter values given in Tables 1, 2 and 4 and using a computational method discussed previously (6). The parameters have not been thoroughly optimized to date but the overall behavior of the model is very encouraging.

Predicted values for void swelling, network dislocation density and faulted loop density are shown in Figure 3, a-c as a function of temperature at two doses for 20% cold-worked material. A comparison with fast reactor data is provided in Figs. 4–6. Values of these key microstructural features are well tracked by the model over this fairly broad temperature range. The swelling data shown in Fig. 4 is from the RS-1 experiment in the Experimental Breeder Reactor-II (EBR-II) (40,41). This experiment included several heats of AISI 316 stainless steel which had been developed to meet the specifications for components in the first core of the Fast Flux Test Facility (FFTF). The temperatures shown in Fig. 4 reflect a downward revision from the original design

temperatures (42). The model predicts both incubation times and peak swelling rates (~1%/dpa in the peak swelling region) which are similar to the data. The model predictions of swelling at temperatures greater than 650°C in Fig. 3a are also consistent with recent observations (41).

There is much less data with which to compare the model's predictions of dislocation and faulted loop densities. Figure 5 compares dislocation densities for M316 stainless steel irradiated in the Dounreay Fast Reactor and the DO-heat of 316 stainless steel irradiated in the EBR-II (27,43). The agreement is quite good. The results are also consistent with other reported values for AISI 316 stainless steel irradiated in the EBR-II (43). Predicted faulted loop densities are compared with data from several sources in Fig. 6. The data are for AISI 316 stainless steel irradiated in both the solution annealed and cold-worked conditions at doses between about 6 and 16 dpa (28,44–47). The data from Ref. 27 includes varying stress levels. The predicted curves reflect the peak faulted loop density for both solution annealed and 20% cold worked starting conditions. The data is reasonably well represented by the predictions except at low temperatures where the loop density is somewhat low.

The fluence dependence of the model predictions at 500°C is shown in Fig. 7a and 7b for 20% cold worked and solution annealed material, respectively. The coupling of the evolution of the various microstructural features is clearly seen. After an initial transient the microstructure reaches a state which is independent of the initial condition. The incubation time for swelling is not primarily associated with the dislocation transient but rather with the time required for the cavities to accumulate the critical number of helium atoms

(3–8). Following the initiation of void swelling, additional recovery occurs as the cavity sink strengths begins to increase. A regime in which the swelling rate is approximately constant and fairly high occurs when the cavity and dislocation sink strengths have similar values. When such parity occurs the maximum theoretical swelling rate is observed (48). Although it is not shown in Fig. 7, at high doses the cavity sink strength exceeds the dislocation sink strength and the swelling rate begins to decrease as predicted by theory (48). The precise coincidence of the values for the solution annealed and cold-worked material at such low doses may be somewhat artificial. The model does not include an explicit cavity nucleation calculation and the same initial cavity densities were used for both materials. Some data indicates that void densities at low doses are higher for solution annealed material (46) and neglecting this difference may influence the model's predictions at low doses.

The evolution towards a saturation microstructure has been observed (49,50) and has been discussed elsewhere (1). The predicted low dose peak in the faulted loop number density in solution annealed material has also been observed (46); however, Brager and Straalsund have reported similar high values at low doses in 20% cold worked stainless steel (51) in conflict with the predictions shown in Fig. 7. While the initial recovery of the network dislocation density in the 20% cold-worked material appears to be in agreement with the available data (49,51), the initial transient appears to occur too quickly in the solution annealed material (49). The thermal dislocation source term may be the cause of the too rapid buildup of the network dislocation density for the solution annealed simulation. The source density (S_D) values were developed for 20%

cold-worked material and implicitly reflect a near steady state value for the network dislocation density as discussed above. Hence for the solution annealed material, the values of S_D may be too high at low doses. Explicit dislocation density dependence in S_D may be required to improve the agreement with the solution annealed data.

SUMMARY

The theoretical model described herein provides a vehicle for studying the evolution of the important microstructural features in fast neutron irradiated stainless steel. A prominent feature of the model is a new description of dislocation evolution in which Frank faulted loops nucleate, grow, and unfault to provide a source for network dislocations while network dislocations are simultaneously annihilated by climb/glide processes. Faulted loop evolution is simulated using a novel scheme in which discrete cluster equations are used to describe the smallest loops and a discretized continuum distribution is used to describe the larger loops. It has been shown by a rigorous analysis that the joining of these two quite different descriptions is self-consistent when the prescription applied here is followed. This scheme greatly reduces the number of equations necessary to describe the loop distribution. The model also includes components which describe the evolution of the dislocation network in the absence of irradiation. This dislocation evolution model has been linked with a previously developed model of cavity evolution which had been used to analyze the problem of void swelling (5,7).

The predictions of the model indicate that the individual features do not evolve independently but are coupled via their mutual influences on the point

defect concentrations. Although the model incorporates the time dependence of only three major microstructural components (cavities, faulted loops, and network dislocations), good agreement has been obtained with a variety of experimental data. It was encouraging to note that as more microstructural features were added to the current model, the parameter space in which one could obtain "reasonable" results became more limited. Even fairly small changes in parameters such as certain of the activation energies could not be accommodated without significantly altering the predictions. This appears to indicate the robustness of the rate theory as a tool for investigating radiation effects and suggests that the relative importance of microstructural evolution may be greater than that of effects such as microchemistry (52). While microchemical changes are known to occur, their effect may be obscured globally by the use of the various rate theory parameters which are effective averages over times and distances greater than the scale of the microchemical variations. In such a case the role of microchemistry may be primarily to influence microstructural evolution.

REFERENCES

1. G. R. Odette, J. Nucl. Mater. 85&86 (1979) 533–545.

2. G. R. Odette, P. J. Maziasz, and J. A. Spitznagel, J. Nucl. Mater. 103&104 (1981) 1289–1304.

3. H. R. Brager and F. A. Garner, "Dependence of Void Formation in Phase Stability in Neutron Irradiated Stainless Steel," Effects of Radiation on Structural Materials: Ninth Int. Symp., ASTM STP 683, ASTM, 1979, 207–232.

4. G. R. Odette and S. C. Langley, Radiation Effects and Tritium Technology for Fusion Reactors, CONF-750989, 1975, I: 395–416.

5. R. E. Stoller and G. R. Odette, J. Nucl. Mater. 103–104 (1981) 1361–1365.

6. G. R. Odette and R. E. Stoller, J. Nucl. Mater. 122&123 (1984) 514–519.

7. R. E. Stoller and G. R. Odette, "The Effect of Helium on Swelling in Stainless Steel: Influence of Cavity Density and Morphology," Effects of Radiation on Materials: Eleventh Int. Symp., ASTM STP 782, ASTM, 1982, 275–294.

8. R. E. Stoller and G. R. Odette, J. Nucl. Mater. 131 (1985) 118–125.

9. L. K. Mansur and W. A. Coghlan, J. Nucl. Mater. 119 (1983) 1–25.

10. M. R. Hayns, The Transition From Gas Bubble to Void Growth, AERE-R8806, U.K.A.E.A., 1977.

11. K. C. Russell, Acta Met. 26 (1978) 1615–1630.

12. A. D. Brailsford and R. Bullough, The Theory of Sink Strengths, AERE Harwell Report TP.854, 1980.

13. R. A. Johnson, J. Nucl. Mater. 83 (1979) 147–159.

14. O. Dimitrov and C. Dimitrov, J. Nucl. Mater. 105 (1982) 39–47.

15. J. T. Stanley and J. R. Cost, J. Phys. F: Met. Phys. 14 (1984) 1801–1810.

16. H. Saka, Phil. Mag. 42 (1980) 185–194.

17. J. P. Hirth, and J. Lothe, Theory of Dislocations, McGraw-Hill, New York, 1968.

18. Materials Handbook for Fusion Energy Systems, DOE/TIC-10122, U.S. Department of Energy, Office of Fusion Energy.

19. R. E. Stoller and G. R. Odette, "Microstructural Evolution in an Austenitic Stainless Steel Fusion Reactor First Wall," Proc. of Second International Conference on Fusion Reactor Materials, Chicago, Ill., April 14–19, 1986, to be published in J. Nucl. Mater.

20. F. R. N. Nabarro, Phil. Mag. 16 (1967) 231–237.

21. J. Gittus, Creep, Viscoelasticity and Creep Fracture in Solids, John Wiley and Sons, New York, 1975.

22. W. D. Nix, R. Gasca-Neri, and J. P. Hirth, Phil. Mag. 23 (1971) 1339–1349.

23. G. B. Gibbs, Phil. Mag. 23 (1971) 771–780.

24. J. Bardeen and C. Herring, Imperfections in Nearly Perfect Crystals, W. Schockley (Ed.), John Wiley and Sons, New York, 1952.

25. D. Fahr, E. E. Bloom, and J. O. Stiegler, "Irradiation Embrittlement and Creep in Fuel Cladding and Core Components," Proc. of BNES Conf., London, 1972, 167–177.

26. G. D. Johnson, F. A. Garner, H. R. Brager, and R. L. Fish, "A Microstructural Interpretation of the Fluence and Temperature Dependence of the Mechanical Properties of Irradiated AISI 316," Effects of Radiation on Materials: Tenth Int. Symp., ASTM STP 725, ASTM, 1981, 393–412.

27. P. J. Maziasz, Alloy Development for Irradiation Performance, Quarterly Progress Report, DOE/ER-0045/7, 1971, 54–97.

28. H. R. Brager, F. A. Garner, and G. L. Guthrie, J. Nucl. Mater. 66 (1977) 181–197.

29. W. Assassa and Guialdenq, Met. Sci. 12 (1978) 123–128.

30. S. J. Rothman, L. J. Nowicki, and G. E. Murch, J. Physics. F: Metal Phys. 10 (1980) 383–398.

31. L. E. Murr, G. I. Wong, and R. J. Horylev Acta Met. 21 (1973) 593–603.

32. R. E. Schramm and R. P. Reed, Met. Trans. A 6A (1975) 1343–1418.

33. J. J. Sniegowski and W. G. Wolfer, "On the Physical Basis for the Swelling Resistance of Ferritic Steels," Ferritic Alloys for Use in Nuclear Energy Technologies, Proc. of Topical Conf., TMS AIME, New York, 1984.

34. M. R. Hayns, J. Gallagher, and R. Bullough, "The Derivation of a Simple Void Swelling Equation for Cold Worked 316 Austenitic Stainless Steel," AERE Harwell Report TP.739, 1978.

35. P. T. Heald, Phil. Mag. 31 (1975) 551–558.

36. F. W. Young, J. Nucl. Mater. 69&70 (1978) 310–370.

37. L. K. Mansur, J. Nucl. Mater. 83 (1979) 109–127.

38. N. M. Ghoniem and D. D. Cho, "The Influence of Vacancy Clustering on the Early Stages of Interstitial Loop Formation and Growth," UCLA-ENG-7845, School of Engineering and Applied Science, University of California, Los Angeles, 1978.

39. M. R. Hayns, J. Nucl. Mater. 56 (1975) 267–274.

40. J. F. Bates and M. K. Korenko, Nucl. Tech. 48 (1980) 303–314.

41. F. A. Garner, "Overview of the Swelling Behavior of 316 Stainless Steel," Optimizing Materials for Nuclear Applications, Symp. Proc., TMS AIME, New York, 1985.

42. R. W. Clark, "Dimensional Change Correlations for 20% Cold-Worked AISI 316 Stainless Steel for Fusion Applications," Master's Degree Thesis, University of Missouri, Rolla, 1985.

43. J. I. Bramman, C. Brown, J. S. Watkin, C. Cawthorne, E. J. Fulton, P. J. Barton, and E. A. Little, "Void Swelling and Microstructural Changes in Fuel Pin Cladding and Unstressed Specimens Irradiated in DFR," Radiation Effects in Breeder Reactor Structural Materials, Int. Conf. TMS AIME, New York, 1977, 479–507.

44. H. R. Brager and J. L. Straalsund, J. Nucl. Mater. 46 (1973) 124–158.

45. P. J. Barton, B. L. Eyre, and D. A. Stow, J. Nucl. Mater. 67 (1977) 181–197.

46. H. R. Brager, J. Nucl. Mater. 57 (1975) 103–118.

47. E. E. Bloom and J. O. Stiegler, Effects of Irradiation on Substructure and Mechanical Properties of Metals and Alloys, ASTM STP 529, ASTM, 1973, 360–382.

48. L. K. Mansur, Nucl. Tech. 40 (1978) 5–34.

49. H. R. Brager, F. A. Garner, E. R. Gilbert, J. E. Flinn, and W. G. Wolfer, J. Nucl. Mater. 46 (1973) 727–756.

50. N. H. Packan and K. Farrell, "Ion Damage in 316 Stainless Steel Over a Broad Dose Range," Effects of Radiation on Materials: Eleventh Int. Symp. ASTM STP 782, 1982, 885–894.

51. H. R. Brager and J. L. Straalsund, J. Nucl. Mater. 47 (1973) 105–109.

52. F. A. Garner, "The Microchemical Evolution of Irradiated Stainless Steel," Phase Stability During Irradiation, Symp. Proc., TMS AIME, New York, 1981, 165–190.

TABLE 1--Variable Definitions

Parameter	Value/Units
Lattice parameter, a_o	3.58×10^{-10} m
Atomic volume, Ω	1.15×10^{-29} m^3 ($a_o^3/4$)
Network dislocation Burgers vector magnitude, b_d	2.53×10^{-10} m ($a_o/\sqrt{2}$)
Faulted loop Burgers vector magnitude, b_ℓ	2.07×10^{-10} m ($a_o/\sqrt{3}$)
Vacancy diffusivity, D_v	m^2/sec
Interstitial diffusivity, D_i	m^2/sec
Vacancy concentration, C_v	#/atom
Thermal equilibrium vacancy concentration, C_v^e	#/atom
Interstitial concentration, C_i	#/atom
Di-interstitial concentration, C_2	#/atom
Tri-interstitial concentration, C_3	#/atom
Tetra-interstitial concentration, C_4	#/atom
Extended defect sink strengths, $S_{i,v}^j$	m^{-2}
Extended defect equilibrium vacancy concentrations, C_v^j	#/atom

where: j = c for cavities

= n for network dislocations

= ℓ for faulted loops

= g for subgrains

= vcl for microvoids

TABLE 2. Typical Material and Input Parameters

Parameter	Value
Vacancy migration energy, E_v^m	1.4 eV
Vacancy formation energy, E_v^f	1.6 eV
Interstitial migration energy, E_i^m	0.85 eV
Di-interstitial binding energy, E_2^b	1.35 eV
Tri-interstitial binding energy, E_3^b	1.75 eV
Helium-divacancy binding energy, E_{He}^b	0.5 eV
Vacancy diffusivity pre-exponential, D_v^o	8.0×10^{-5} m^2/sec
Interstitial diffusivity pre-exponential, D_i^o	8.0×10^{-6} m^2/sec
Recombination coefficient, α	2×10^{17} D_i sec^{-1}
Displacement rate, G_{dpa}	1×10^{-6} dpa/sec
Helium generation rate, G_{He}	3.50×10^{-13} He/atom/sec
Cascade efficiency, η	0.333
Fraction of cascade vacancies collapsed into microvoids, χ	0.6
Interstitial/vacancy combinatorial number for interstitial clusters	$Z_i^1 = 63$ $Z_v^2 = 33$ $Z_i^2 = 90$ $Z_v^3 = 38$ $Z_i^3 = 110$ $Z_v^4 = 42$ $Z_i^4 = 130$
Surface free energy, γ	$3.24 - 1.4 \times 10^{-3}$ T(°C) J/m^2
Stacking fault energy, γ_{sf}	1.5×10^{-2} J/m^2
Initial dislocation density, $\rho_n(0)$	3.0×10^{15} m^{-2} - 20% cold worked 3.0×10^{13} m^{-2} - solution annealed
Network dislocation/interstitial bias, Z_i^n	1.25
Faulted loop/interstitial bias, Z_i^ℓ	1.50

Table 2 (Continued)

Parameter	Value
Subgrain size, d_g	$T \leq 500°C$ 1.0×10^{-6} m $= 550$ 1.25×10^{-6} m $= 600$ 3.0×10^{-6} m $= 650$ 7.75×10^{-6} m $= 700$ 1.70×10^{-5} m
Microvoid radius, r_{mv}	$T = 350°C$ 7.0×10^{-10} m $= 400°C$ 7.5×10^{-10} m $\geq 450°C$ 8.0×10^{-10} m
Total cavity density, N_c^t	$2.53 \times 10^{26} \exp(-0.023\ T(°C))$ m$^-$
Precipitate associated cavity fraction, f_p	0.1
Precipitate sink strength, S_p	4×10^{14} m^{-2}
Precipitate nucleation time, τ_p	$0.16\ (700 - T(°C))$ dpa
	matrix ppt. associated
Cavity volume factor, $3F_v(\beta)/4\pi$	1.0 0.40
Cavity surface area factor, $F_s(\beta)/4\pi$	1.0 0.434

TABLE--3 Results of thermal dislocation evolution calibration

Dislocation Density Ratio: $\frac{\text{Cold Worked + 4000 h at T}}{\text{As Cold Worked}}$

Test Temperature T (°C)	Data	Model
450	0.73	0.99
550	0.41	0.41
650	0.054	0.053

TABLE--4 Thermal dislocation evolution parameters

Modified back stress term, A' 0.05

Temperature	Source density, S_D
550°C	2.0×10^{21} m^{-3}
600°C	9.7×10^{20} m^{-3}
650°C	1.2×10^{20} m^{-3}
700°C	2.0×10^{19} m^{-3}

FIGURE CAPTIONS

FIGURE 1. Faulted loop density (N_1) and loop line length (ρ_1) as a function of the number of loop size classes.

FIGURE 2. Schematic drawing of Bardeen-Herring dislocation source (after Ref. 23).

FIGURE 3. Temperature dependence of model predictions of swelling, network dislocation density and faulted loop density at 50 and 100 dpa.

FIGURE 4. Comparison of predicted swelling and fast reactor data at an intermediate and high fluence (39,40).

FIGURE 5. Comparison of predicted network dislocation density and fast reactor data at 40 dpa (Ref. 25,42).

FIGURE 6. Comparison of predicted faulted loop density and low fluence fast reactor data (27,43–46).

FIGURE 7. Dose dependence of predicted swelling, network dislocation density, ane descriptions for the 500°C for 20% cold worked and solution annealed material.

ORNL-DWG 85-16836

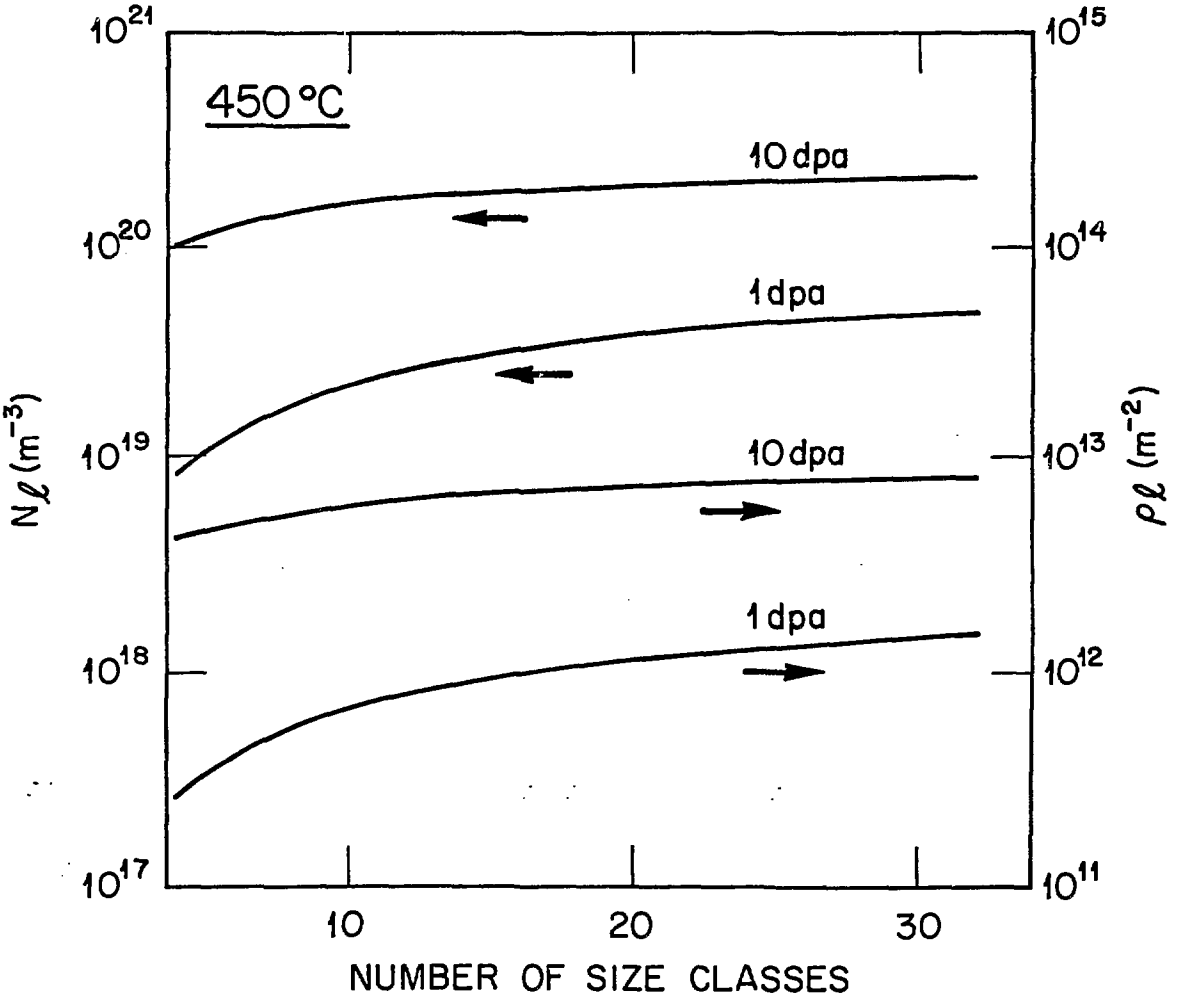

Stoller and Odette, R-145
Fig. 1

ORNL-DWG 85-16835

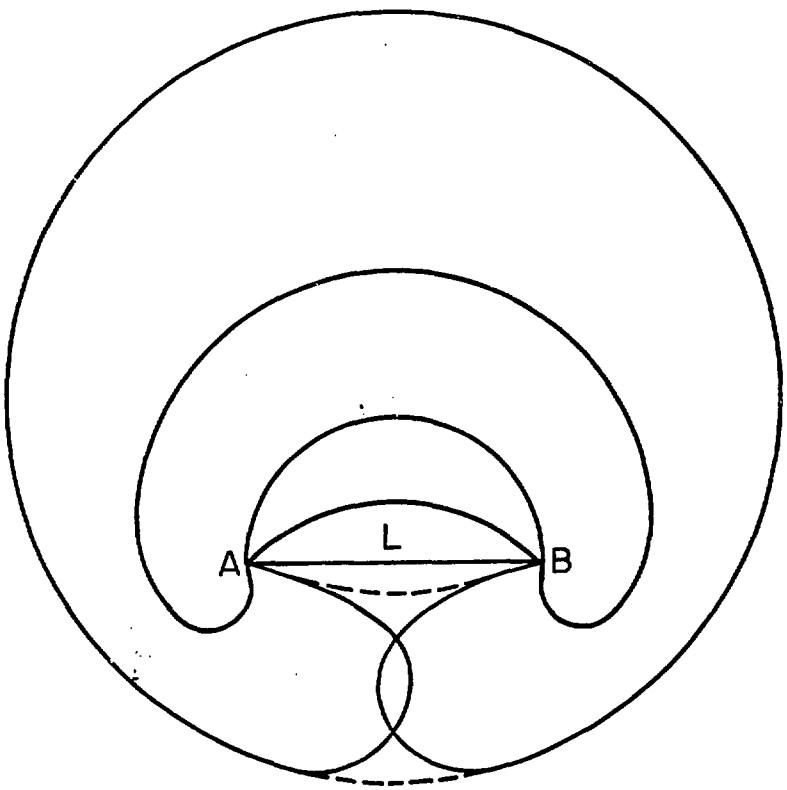

Stoller and Odette
R-145
Fig 2

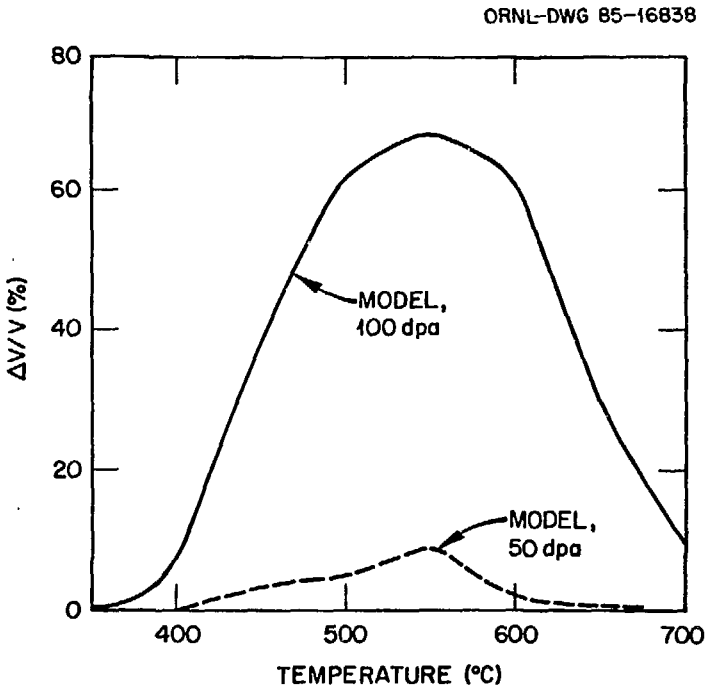

Stiller and Odette
R-145
Fig 3c

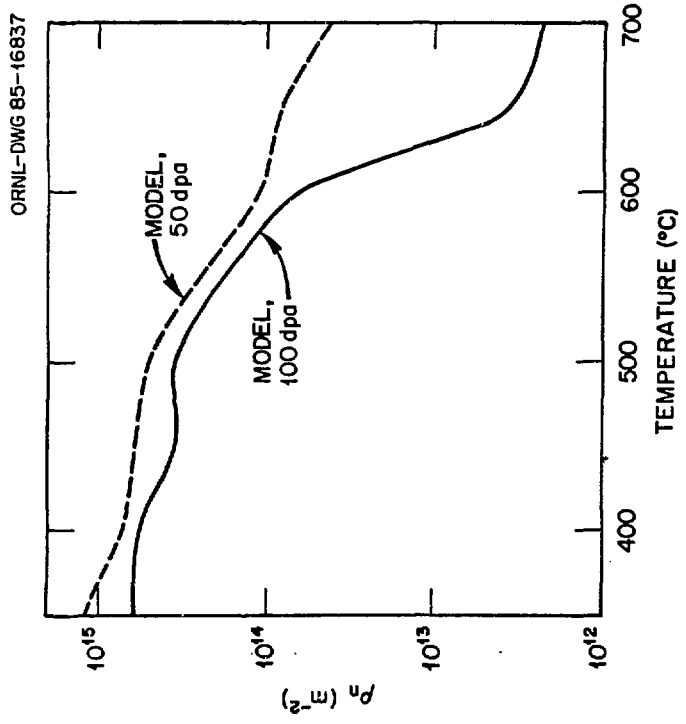

Stoller and Odette
R-145

Fig 36

ORNL-DWG 85-16842

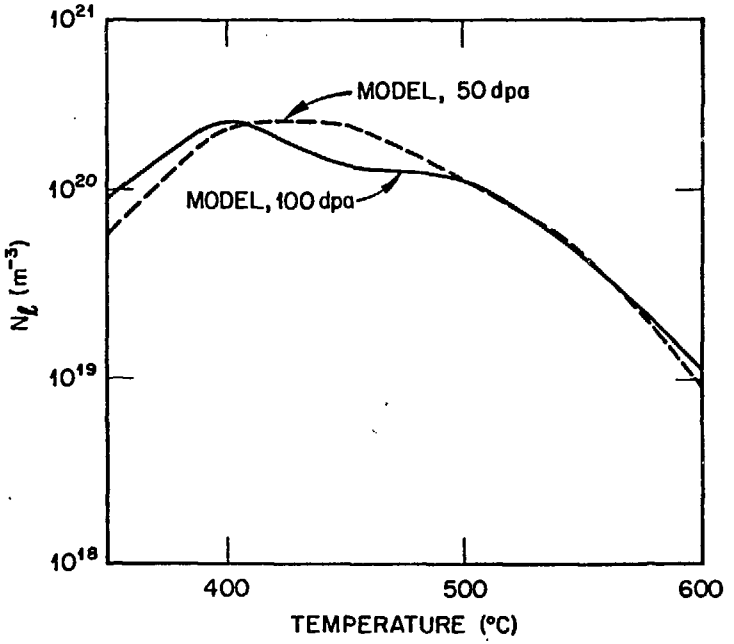

Stoller and Odette
12-145
Fig 3c

ORNL-DWG 85-16844

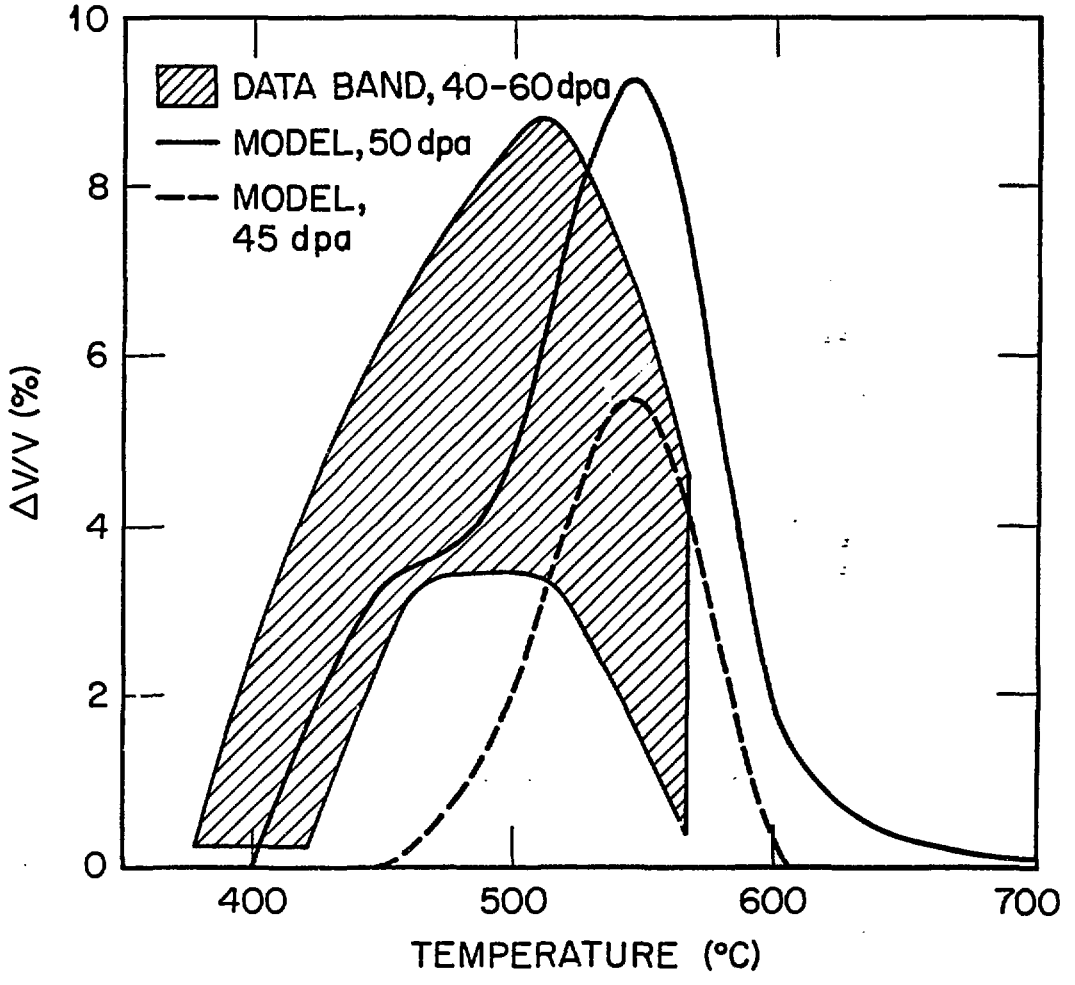

Stoller and Odette
R-145

Fig 4a

ORNL-DWG 85-16845

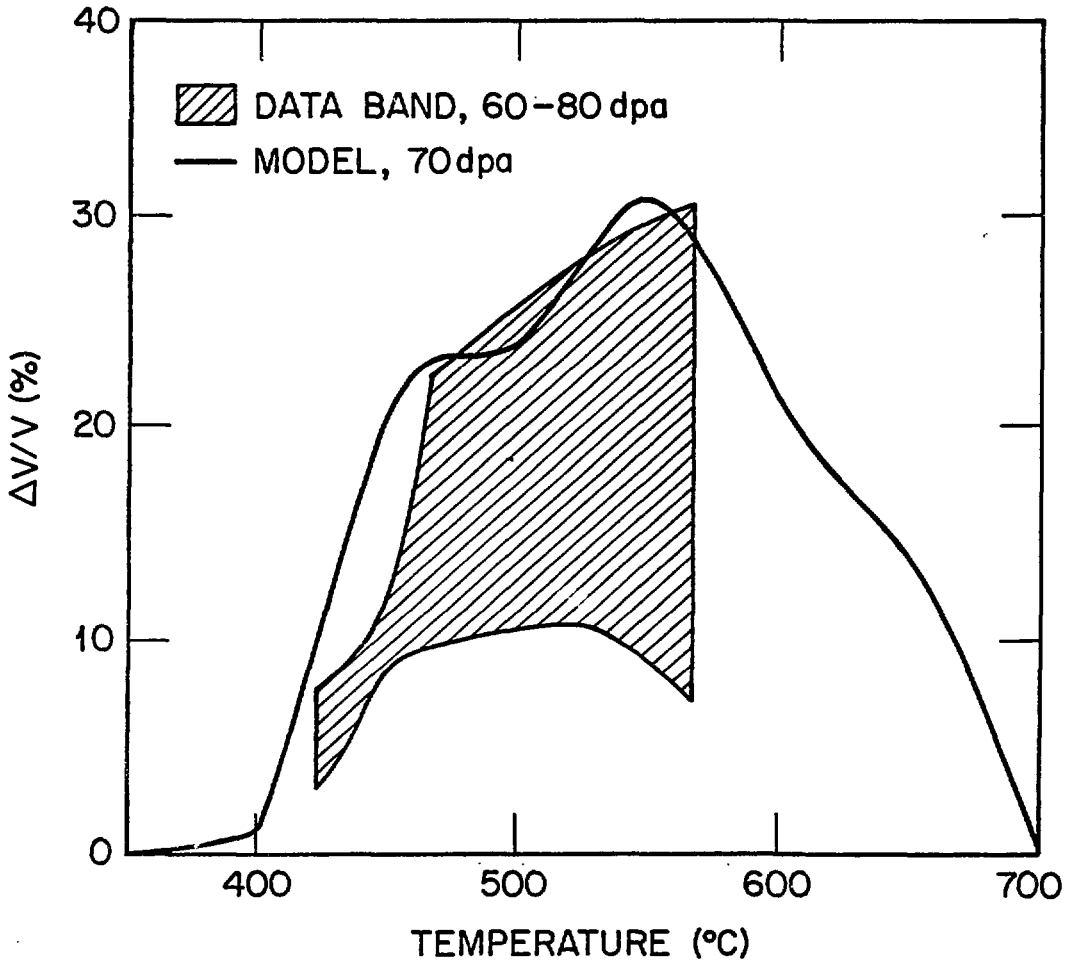

Stoller and Odette
R-145
7g4b

ORNL-DWG 85-16843R

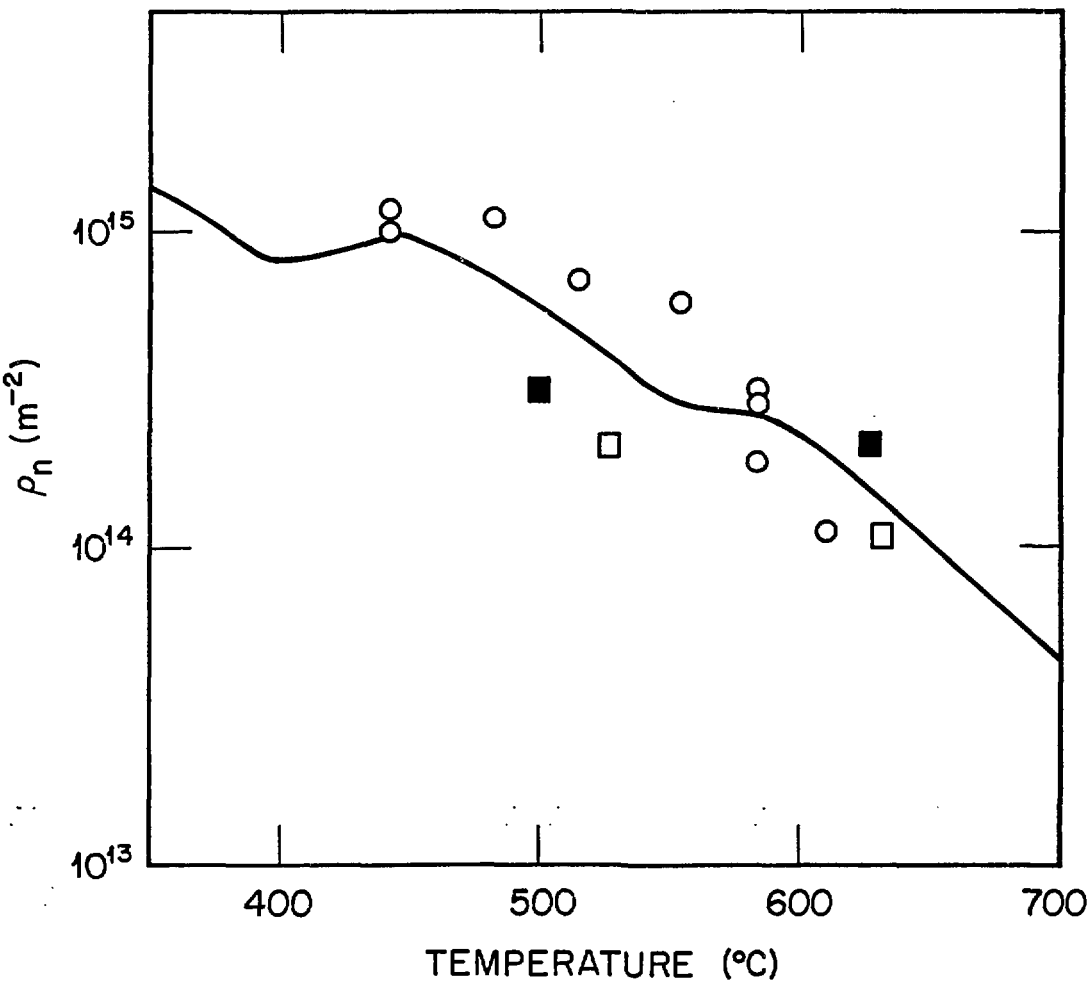

■ 8.4 dpa
□ 36 dpa
} PJM (DOE/ER-0045/7, 1981)

○ 29-40 dpa JIB, et al. (Rad. Effects in Breeder Reactor Structural Materials, 1977)

—— MODEL, 40 dpa

Stoller and Odette
R-145
Fig. 5

ORNL-DWG 85-17824R

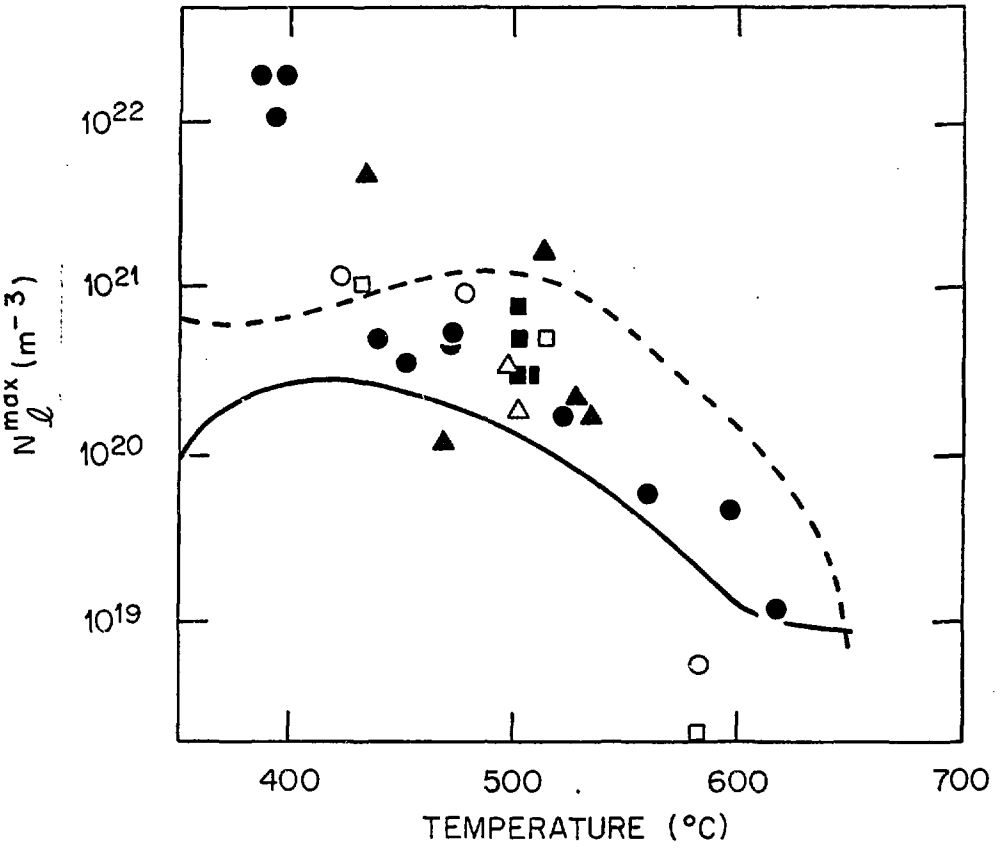

——— MODEL, $\rho_n(0) = 3 \times 10^{15}$ m^{-2}

– – – MODEL, $\rho_n(0) = 3 \times 10^{13}$ m^{-2}

● HRB AND JLS (JNM 46), SA 316

▲ PJB, BEL AND DAS (JNM 67), SA 316

○ HRB (JNM 57), CW 316

△ HRB, FAG AND GLG (JNM 66), CW 316

■ HRB, FAG AND GLG (JNM 66), SA 316

□ EEB AND JOS (ASTM STP 529), SA 316

Stoller and Odette
R-145
Fig. 6

ORNL-DWG 85-16839

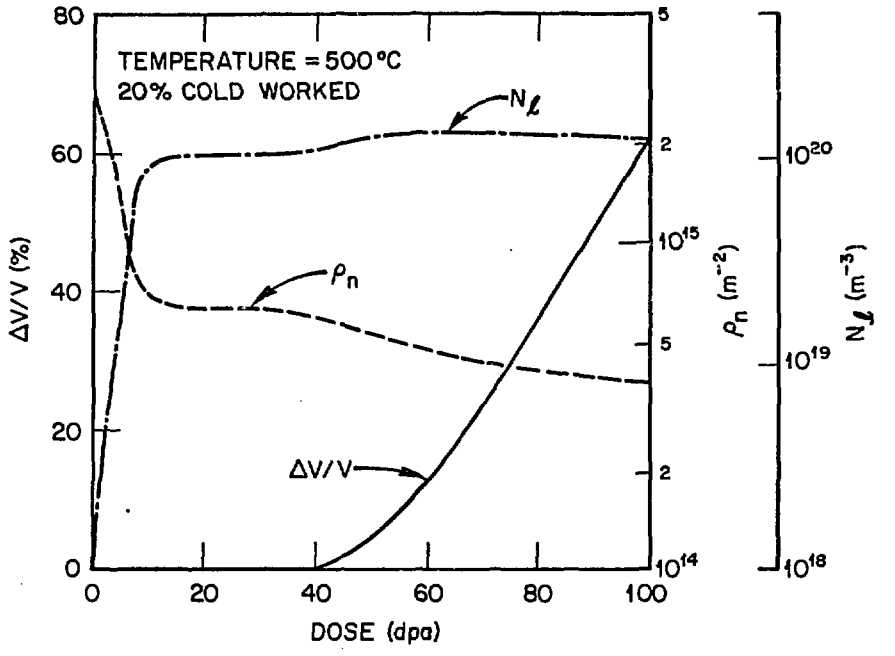

ORNL-DWG 85-16840

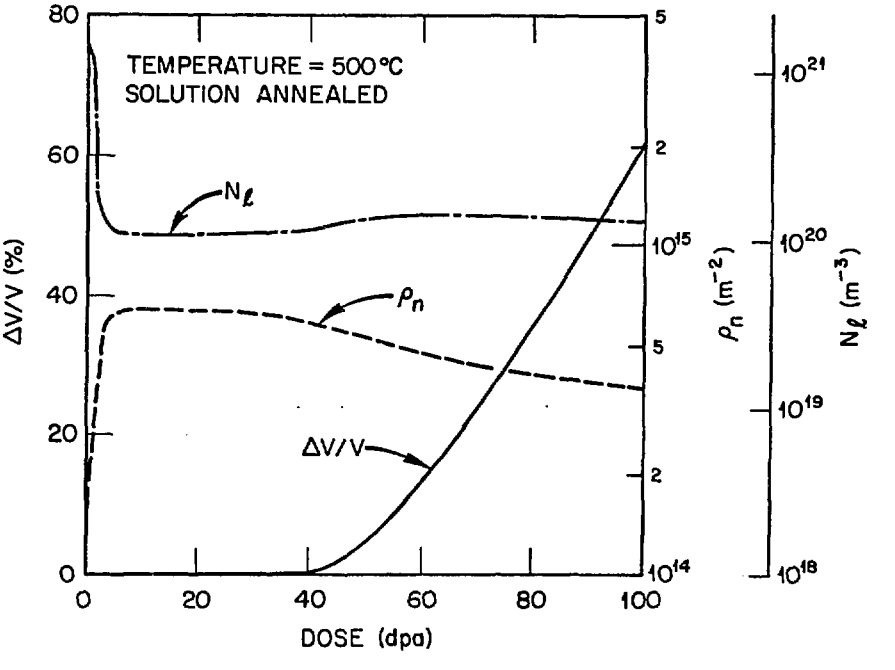

DISCLAIMER

This report was prepared as an account of work sponsored by an agency of the United States Government. Neither the United States Government nor any agency thereof, nor any of their employees, makes any warranty, express or implied, or assumes any legal liability or responsibility for the accuracy, completeness, or usefulness of any information, apparatus, product, or process disclosed, or represents that its use would not infringe privately owned rights. Reference herein to any specific commercial product, process, or service by trade name, trademark, manufacturer, or otherwise does not necessarily constitute or imply its endorsement, recommendation, or favoring by the United States Government or any agency thereof. The views and opinions of authors expressed herein do not necessarily state or reflect those of the United States Government or any agency thereof.

Stoller and Odette
R-145
Fig 7a, 7b